Velocity Profiles in a Baffled Vessel with Single or Double Pitched-Blade Turbines

Piero M. Armenante and Chun-Chiao Chou
Dept. of Chemical Engineering, Chemistry, and Environmental Science, New Jersey Institute of Technology, Newark, NJ 07102

A laser-Doppler velocimetry (LDV) apparatus and a computational fluid dynamic (CFD) software package (FLUENT) were used to experimentally determine and numerically predict the velocities in a baffled vessel agitated by one or two 45° pitched-blade turbines. The flow characteristics in the impeller regions were measured by LDV and used as boundary conditions in the numerical computations. Turbulence effects were simulated using either the k-ϵ model or algebraic stress model (ASM). The CFD predictions were compared to the LDV measurements in terms of average velocities in all three directions as well as turbulent kinetic energies. Predictions based on ASM were typically in closer agreement with the experimental data than those based on the k-ϵ model. Flow patterns in both configurations were dominated by the axial and tangential components. The presence of the upper impeller altered the flow considerably, producing a strong vertical recirculation pattern between the impellers and significantly reducing the circulation flow below the lower impeller.

Introduction

Mixing vessels provided with pitched-blade turbine (PBT) agitators are commonly found in a variety of industrial applications. Because of the strong axial flow component that they generate, PBTs are often used in a variety of process operations, such as solid suspension off the bottom of vessels. The flow produced by a downpumping PBT is a complex one, typically involving the generation of a jet directed at an angle from the impeller, impinging the vessel bottom at a location halfway between the center of the vessel and the wall (Fort, 1986).

In recent years the flow distribution in agitated vessels has been studied primarily using two complementary techniques, laser-Doppler velocimetry (LDV) and computational fluid dynamics (CFD) simulations. These two tools have enabled investigators to experimentally and nonintrusively determine the velocity distribution in mixing vessels, and make quantitative predictions about the same velocities (Mahouast et al., 1989; Costes et al., 1991; Hirata et al., 1991; Jaworski et al., 1991; Weetman, 1991; de Groot, 1991; Bakker, 1992; Kresta and Wood, 1991; Ranade et al., 1989, 1992; Dyster et al., 1993). A few of these studies were focused on the flow generated by a single PBT in a mixing vessel (Ranade and Joshi, 1989; Ranade et al., 1989, 1992; Jaworski et al., 1991; Kresta and Wood, 1993a,b). Of these investigations, some were focused on LDV measurements of velocity components (Jaworski et al., 1991; Kresta and Wood, 1993a,b), and others examined primarily the flow predictions based on CFD simulations (Ranade et al., 1989). Although studies have been conducted in which quantitative comparisons between LDV and CFD results for radial impellers were produced (Luo et al., 1993; Ranade and Joshi, 1990a,b), only two studies could be found in the literature for the case of PBTs.

A limitation of previous CFD studies on PBTs has been the use of only one turbulence model (k-ϵ) in the simulations, and the specification of the boundary conditions in the impeller region at only one location (typically the bottom surface of the volume swept by the impeller). An additional limitation has been the use of only a single impeller. However, in many industrial applications multiple impellers are used. The presence of additional impellers in the mixing vessel typically results in significant flow changes with respect to the flow pattern generated by a single impeller. This can have beneficial effects on some aspects of the process (by increasing the power per unit liquid volume delivered to the fluid), but can

Correspondence concerning this article should be addressed to P. M. Armenante.

also have unexpected results, such as a less efficient solid suspension or liquid–liqiud dispersion, for some design configurations (Armenante et al., 1992; Armenante and Li, 1993).

Therefore, the primary objective of the present investigation was to map the velocity distribution inside a mixing vessel via LDV and to use the experimental data so obtained to determine the validity of the CFD simulation. This approach was used to study both single-PBT and double-PBT agitation systems. In addition, the simulations were carried out with two different turbulence models, and, for the single-PBT configuration, three different sets of boundary conditions were also used in the impeller region. Furthermore, this investigation was carried out using a PBT that projected a blade width-to-impeller diameter ratio (1/8) commonly used in industry but not typically studied in previous CFD or LDV investigations.

Numerical Simulation

Numerical simulations were conducted to determine the velocity profiles inside the vessel. A commercial CFD finite volume software package (FLUENT, version 3.03) was used for this purpose. The numerical technique used by this program involves the subdivision of the domain of interest into a finite number of control volumes and the discretization of the steady-state, time-averaged continuity and momentum equations in the turbulent regime to obtain simultaneous algebraic equations, then solved iteratively (Creare.x, 1990).

Both the k-ϵ model and the algebraic stress model (ASM) were used to account for turbulence effects. Accordingly, the Reynolds stresses $\rho\overline{u'u'}$ were modeled, respectively, as

$$\overline{u_i'u_j'} = \frac{2}{3}\delta_{ij}k - \frac{\mu_t}{\rho}\left(\frac{\partial \bar{u}_i}{\partial x_j} + \frac{\partial \bar{u}_j}{\partial x_i}\right)$$

or

$$\overline{u_i'u_j'} = \frac{2}{3}\delta_{ij}k + \frac{C_D}{(p/\epsilon) - 1 + C_3'}\frac{k}{\epsilon}\left(p_{ij} - \frac{2}{3}p\delta_{ij}\right), \quad (1)$$

where (Creare.x, 1990; Launder and Spalding, 1972):

$$p = \frac{1}{2}p_{ii} \quad \text{and} \quad p_{ij} = -\overline{u_i'u_l'}\frac{\partial \bar{u}_j}{\partial x_l} - \overline{u_j'u_l'}\frac{\partial \bar{u}_i}{\partial x_l}. \quad (2)$$

The turbulent viscosity was obtained from (Rodi, 1984):

$$\mu_t = \rho C_\mu \frac{k^2}{\epsilon}. \quad (3)$$

The values of the specific turbulence kinetic energy, k, and the turbulence energy dissipation rate, ϵ, were obtained from their balance equations:

$$\boldsymbol{u}\cdot\nabla k = \nabla\left[\left(\frac{\mu_t}{\rho\sigma_k}\right)\nabla k\right] + \frac{G_k}{\rho} - \epsilon \quad (4)$$

$$\boldsymbol{u}\cdot\nabla\epsilon = \nabla\left[\left(\frac{\mu_t}{\rho\sigma_\epsilon}\right)\nabla\epsilon\right] + C_1'\frac{\epsilon}{k}\frac{G_k}{\rho} - C_2'\frac{\epsilon^2}{k}, \quad (5)$$

where

$$k = \frac{1}{2}(\boldsymbol{u}'\cdot\boldsymbol{u}') \quad (6)$$

and

$$G_k = -\rho\overline{\boldsymbol{u}'\boldsymbol{u}'}:(\nabla\boldsymbol{u}). \quad (7)$$

The values of the constants C_1', C_2', C_3', C_D, C_μ, σ_k, and σ_ϵ were taken to be equal to 1.44, 1.92, 0.55, 0.45, 0.09, 1.0, and 1.3, respectively (Rodi, 1984).

The boundary conditions imposed on the systems were as follows. The boundary conditions at the impeller shaft and at the vessel cylindrical wall, baffles, and horizontal bottom were those derived assuming the no-slip condition. This implied that the shear stress near the solid surfaces was specified using wall functions and that equilibrium between the generation and dissipation of turbulence energy was assumed (Launder and Spalding, 1974; Ranade et al., 1989). The boundary conditions at the top (free surface) were of the zero-gradient, zero-flux type, which is equivalent to a frictionless impenetrable wall. The vessel was assumed to be symmetric along its axis and the impeller centerline. This implied that at the vessel axis the radial and tangential velocities and the gradients of the axial velocity and turbulent kinetic energy were all imposed to be zero in the fluid (Ranade et al., 1989; Creare.x, 1990).

In the single-PBT simulation runs, the boundary conditions in the impeller region were imposed at one or more of the surfaces of the cylinder having the same size of the volume swept by the impeller. In particular, one of three different sets of boundary conditions (named BC #1, BC #2, and BC #3, respectively) was imposed in any given simulation. When BC #1 was used, the time-averaged tangential and axial fluid velocities at the bottom surface of the region swept by the impeller(s) were specified, while all the other cells (including those in the impeller volume) were treated as "live" cells whose velocities were determined by the simulation. The k values along the same surface were also specified, as well as the corresponding values of ϵ, calculated from

$$\epsilon = \alpha\frac{k^{1.5}}{w}, \quad (8)$$

where α was taken to be equal to 1.4 (Wu and Patterson, 1989; Armenante et al., 1994). The boundary time-averaged velocities and the fluctuating velocities necessary to calculate k were experimentally determined using the LDV system, as described below. Similarly, when BC #2 was used, the tangential and axial velocities and the corresponding k and ϵ values were specified at the top and bottom surfaces of the impeller region. Finally, BC #3 consisted of a set of boundary conditions at the top and bottom surfaces of the impeller region (identical to BC #2), as well as at the outer vertical cylindrical wall of the volume swept by the impeller. The simulations for the double-PBT agitation systems were always

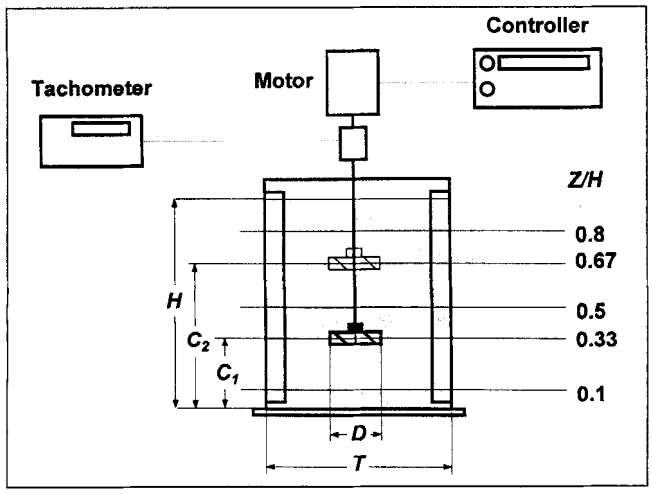

Figure 1. Agitation apparatus.

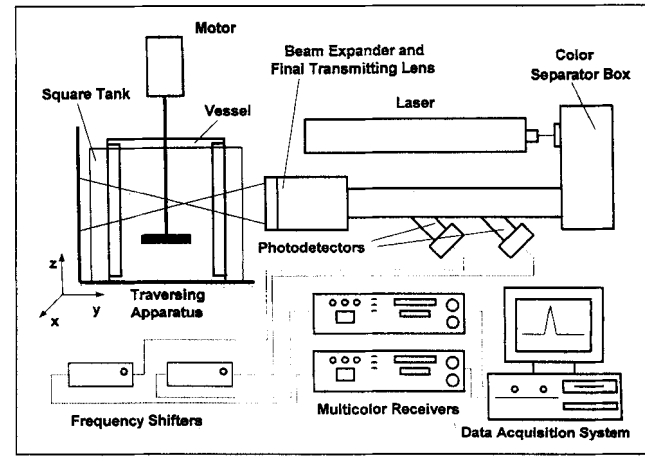

Figure 2. Laser-Doppler velocimetry system.

conducted with BC #2, using as boundary conditions the experimentally obtained velocities for each one of the two impeller regions.

A repeating 90° domain containing 24,696 cells was used in the numerical integration of the preceding equations.

Experimental Apparatus and Method

Figure 1 shows the experimental mixing apparatus. A baffled, cylindrical, flat-bottomed, Plexiglas tank with a diameter of 0.29 m and filled with water (the process fluid in all experiments) up to a height of 0.36 m was used as the mixing vessel. The baffle thickness was 6.25 mm, and the baffle width-to-tank diameter ratio was 0.1. The clearance between the baffles and the tank bottom was 15 mm. The vessel was placed in a square tank, also filled with water, to minimize the effect of diffraction on LDV measurements. The agitation system consisted of either one or two downward-pumping, six-blade, 45° pitched-blade turbines mounted on a centrally located shaft (12.5 mm OD), and with a diameter and a vertically projected blade width equal to 0.102 m and 0.013 m, respectively. The impeller hub was a cylinder 12.5 mm high and 25.4 mm in diameter. In both the single and double impeller configurations one impeller was always mounted 0.12 m from the tank bottom so that the ratio of the off-bottom clearance of the lower impeller (measured from the center of the impeller) to the liquid height, C_1/H, was equal to 0.33. In the two-impeller configuration, a second PBT was mounted 0.24 m from the tank bottom so that the C_2/H ratio was equal to 0.67, and the spacing between the impellers, S, was 0.12 m ($S/D = 1.181$). A 1/8-HP motor controlled by an external controller (G. K. Heller) was used to rotate the impeller at a constant agitation speed of 5 rotations/s (300 rpm), as measured by an optical tachometer.

The LDV apparatus (TSI, Inc.) shown in Figure 2 was used to experimentally obtain the velocity and turbulence intensity profiles inside the vessel. The multicolor beam produced by a 2-W laser (Lexel, Inc.) passed through the prisms, mirrors, and light attenuators contained in the color separation assembly box from which only a green beam and a blue beam emerged. Each beam was split into two parallel beams that were all converged in a small elliptical control volume (maximum diameter, 84 μm) formed by their intersection, 480 mm away from the final converging lens of the optical train and located inside the vessel. The water in the vessel was seeded with 1.5-μm silicon carbide particles capable of scattering light as they traveled through the control volume. The scattered light was collected by the receiving optical assembly working in backscatter mode, and the Doppler shift (directly proportional to the particle velocity) was measured with photodetectors. The system was provided with frequency shifters to measure reverse flow velocities. Sampling time was 0.3 s. The data-acquisition system consisted of multicolor receivers and signal analyzer connected to a computer that converted the Doppler shifts to velocity values, and produced on-line measurements of both average and fluctuating velocities. The LDV system was calibrated with a metal disk rotating at a known velocity; the beams were converged on this disk.

The average and fluctuating velocities at eight radial distances ($2r/T$ equal to 0.11, 0.186, 0.262, 0.338, 0.414, 0.51, 0.62, and 0.841, respectively) and five different heights (Z/H equal to 0.1, 0.33, 0.5, 0.67, and 0.8, respectively) in the mixing vessel were experimentally obtained using an x-y-z traversing apparatus on which the vessel-motor assembly was mounted (Figure 1). Two simultaneous velocity measurements in the two directions perpendicular to the axis of the laser could be taken at any location. To obtain all three velocity components two separate measurements were taken for the same (r,Z) point: one in which the laser axis was oriented perpendicularly to the radius along which the measurement was made (yielding the radial and axial velocity components), and another one in which it was parallel (yielding the tangential and axial velocity components; Armenante et al., 1994).

The average and fluctuating velocities 5 mm above and below the impellers were experimentally determined at seven locations along the impeller radius and at five locations along the impeller blade width at a radial distance 1 mm away from the blade tip. These measurements were used as boundary conditions in the numerical simulations, as well as to verify the closure of the mass balance around the impellers. All measurements were typically taken in duplicate.

The overall power drawn by the impeller was experimentally and independently obtained from a direct measurement of the torque at a known agitation speed. A strain gage

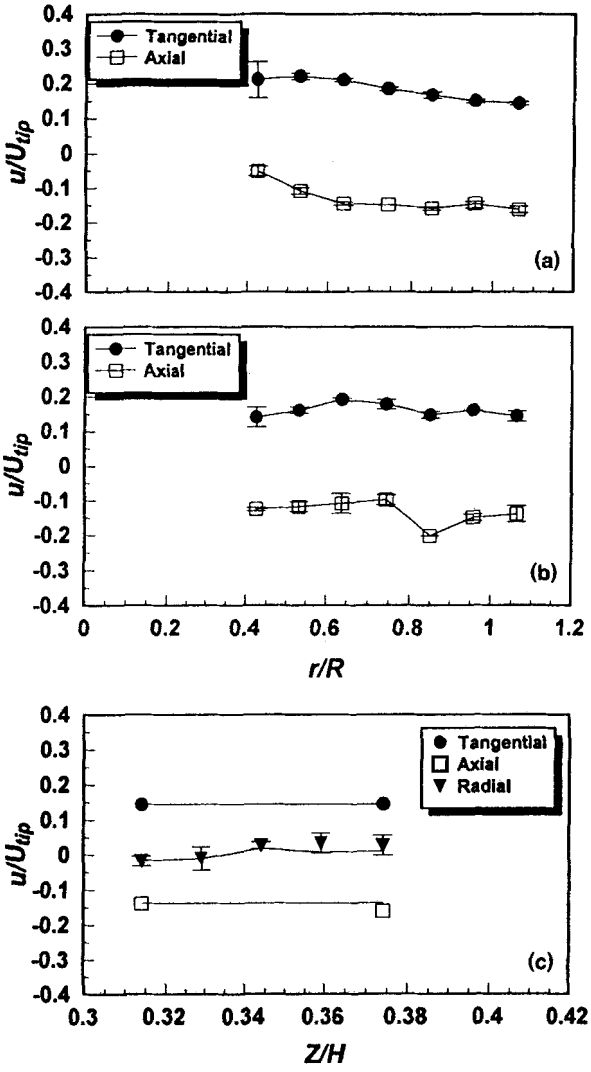

Figure 3. Experimentally determined (via LDV) dimensionless velocities in the impeller region for the single-PBT system.

(a) Velocities at the top plane of the volume swept by the impeller. (b) Velocities at the bottom plane of the volume swept by the impeller. (c) Velocities at the outer vertical cylindrical wall of the volume swept by the impeller. Positive values indicate upward velocities (for the axial direction), or outward velocities (for the radial direction). Error bars indicate standard deviation of duplicate experiments. These velocity values were used as boundary conditions in the CFD simulations (see text).

mounted on a hollow shaft and connected to a data-acquisition system via a slip ring was used for this purpose (Armenante et al., 1992).

Results and Discussion

Single-impeller configuration

Velocities in the Impeller Region. The experimentally determined average axial and tangential velocities in the impeller region are reported in Figure 3. The axial velocities along the top of the impeller were all directed downward, as one would expect for a PBT-induced flow, and nearly constant for r/R values larger than 0.6 (Figure 3a). Closer to the hub the velocities became progressively smaller and approached the zero value. The corresponding velocities on the bottom face of the impeller were constant for $r/R < 0.7$ and became larger in magnitude beyond that point (Figure 3b). The tangential components were relatively constant and similar in magnitude on both faces. The velocities at the outer vertical cylindrical surface of the volume swept by the impeller were also experimentally measured (points in Figure 3c) 1 mm away from the impeller tip.

The velocity profiles in the impeller region observed in this work are flatter than those recently reported by Kresta and Wood (1993b) just below the impeller, or by Ranade et al. (1992) 30 mm below the impeller. On the other hand, the profiles found here are somewhat similar to those reported by Armenante and Chou (1994) and Armenante et al. (1994) for unbaffled systems. Possible explanations for the discrepancies with the results of the previous investigation reported earlier are in the difference in impeller clearance, D/T ratio, and baffling system, since in those studies the baffles extended all the way to the bottom of the vessel, whereas in this work a gap between the baffles and the vessel bottom existed. This could also have an impact on the circulation in the region below the impeller, making it more similar to that found in unbaffled tanks.

The average velocities on all the surfaces of the volume swept by the impeller were used to calculate the flow rate in and out of the impeller region. A mass balance based on the experimental velocities around the impeller indicated that the fluid flow rates entering the top face and leaving from the bottom face were 1.90×10^{-3} m^3/s and 1.78×10^{-3} m^3/s, respectively. When the contribution of the side surface was taken into account, the mass balance could be closed to within 2%, that is, the total outflow from the impeller region was 98% of the total inflow into the same region. By slightly modifying (within the error bars) the radial velocity profile on the side of the volume swept by the impeller, the mass balance around the impeller could be closed to exactly 100%. This modified profile, shown in Figure 3c as a solid line passing within the error bars of the radial velocity points, was used in one of the simulations (based on BC #3) to achieve convergence, as explained below in greater detail.

The velocities in the impeller region were used to calculate the impeller flow number, Fl, from (Jaworski et al., 1991):

$$Fl \equiv \frac{Q}{ND^3}, \tag{9}$$

where Q is the volumetric flow rate discharged from the impeller obtained from

$$Q = 2\pi\int_0^R u_z(r)|_{Z=Z_b} r\,dr + 2\pi R\int_{Z_b}^{Z^+} u_r(Z)|_{r=R}\,dZ, \tag{10}$$

in which the first integral accounts for the flow discharged from the bottom surface of the impeller, and the second integral represents the radial positive flow from the impeller side. In this equation, Z_b is the value of the axial coordinate, Z, at the bottom of the impeller region (in this work, 5 mm below the impeller), and Z^+ is the value of Z up to which the radial flow on the impeller side is directed outwards. The

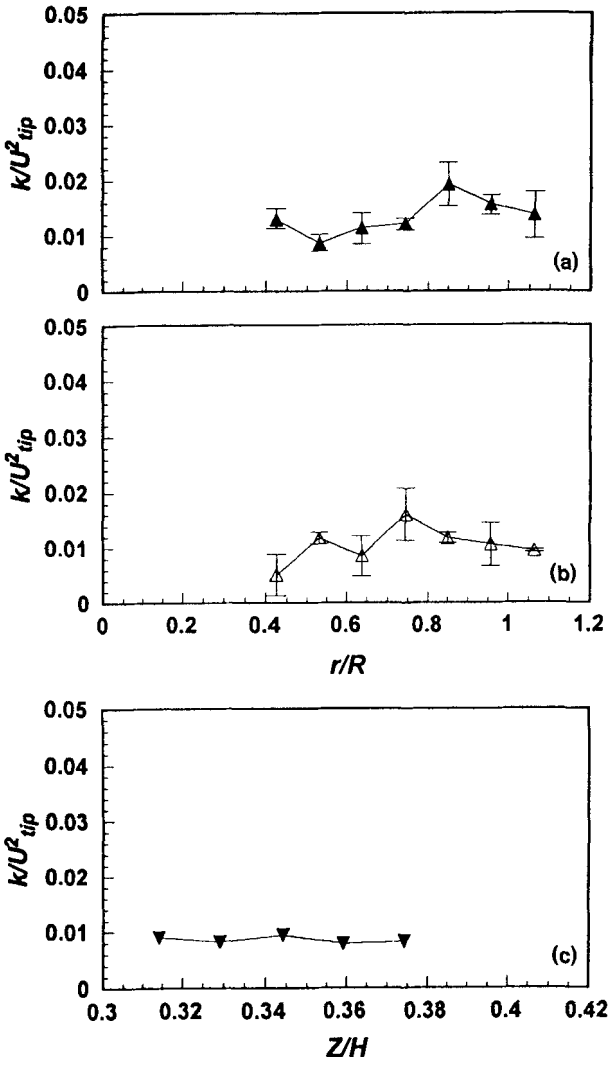

Figure 4. Experimentally determined (via LDV) dimensionless turbulent kinetic energies in the impeller region for the single-PBT system.

(a) Kinetic energies at the top plane of the volume swept by the impeller. (b) Kinetic energies at the bottom plane of the volume swept by the impeller. (c) Kinetic energies at the outer vertical cylindrical wall of the volume swept by the impeller. Error bars indicate standard deviation of duplicate experiments. These kinetic-energy values were used as boundary conditions in the CFD simulations (see text).

second integral was evaluated at a radial distance that was as close to R as possible (in practice, 1 mm) using the experimental LDV velocity measurements as input. In this work the flow number was found to be equal to 0.36. This value is much lower than the values that other investigators have found for PBT, such as 0.71 (Jaworski et al., 1991), 0.753 (Kresta and Wood, 1993b), 0.75–0.79 (Oldshue, 1983, Table 8-3), and 0.85 (Ranada and Joshi, 1989). However, it should be noticed that all these investigators used PBT with a projected blade width-to-impeller diameter ratio (1/5) much larger than that used in this work (1/8). A flow number of 0.85 was also reported by Ranade et al. (1992) using a 45° PBT with a projected blade width-to-impeller diameter of 1/7.07, that is, somewhat similar to that used in this work (1/8). On the other hand, values for Fl similar to that found here have been reported for curved or convex PBTs (0.39; Ranade et al., 1992), or for square pitch propellers (0.4–0.61; Gray, 1966; Oldshue, 1983, Table 8-3). The importance of the w/D ratio can be assessed by examining the data in the literature on power numbers for a PBT with a different blade width. The power number has been reported to be equal to 1.67 for a PBT with a w/D equal ratio of 1/5 (Rewatkar et al., 1990), but only 1.3 for a w/D equal to 1/8 (Bates et al., 1963, 1966).

The fluctuating velocities in all three directions were experimentally determined for the same surfaces in the impeller region and were used to calculate the local turbulence kinetic energy, k. The results are given in Figure 4. The k values shown in Figure 4c for the side of the impeller region were determined using the modified radial velocity profile shown in Figure 3c (instead of the actual experimental points) since these values were later used in BC #3, as explained below. The curves obtained here for k/U^2_{tip} as a function of r/R are flatter than those reported by other investigators (Ranade and Joshi, 1989; Ranade et al., 1992; Kresta and Wood, 1993a), who showed the existence of a peak for k for $r/R \approx 0.5$. However, the results found in the present article are more similar to those obtained in unbaffled vessels (Armenante and Chou, 1994; Armenante et al., 1994).

Velocities Outside the Impeller Region. The values of the three experimentally determined velocity components in the bulk of the fluid were obtained at five vertical and eight radial locations, and are given in Figure 5. The experimental LDV values for the velocities and turbulence kinetic energies in the impeller region (Figures 3 and 4) were used as boundary conditions in the numerical simulations. Initially, all simulations except those based on BC #3 converged (the residual errors of key variables in the simulation eventually dropped to values low enough for convergence to be assumed). The problem of nonconvergence with BC #3 was attributed to the fact that the mass balance around the impeller could not be closed to exactly 100% when the experimental values of the velocities were used as boundary conditions in the simulations. Therefore, the radial velocity profile at the outer vertical cylindrical wall of the volume swept by the impeller was slightly modified so that the mass balance around the impeller could be closed. This profile is shown in Figure 3c as a solid line passing within the error bars of the radial velocity points. When a new simulation based on this modified BC #3 was conducted, convergence was obtained, although the residual errors of one of the variables in the simulation (pressure) remained always higher than in other similar simulations. The results for all the simulations based on different boundary conditions (including the modified BC #3) and different turbulence models are given in Figure 5.

The tangential velocity near the tank bottom ($Z/H = 0.1$) was found to be a weak function of the radial distance (Figure 5). A possible explanation for this is the lack of baffling action in that region caused by the presence of a gap between the baffles and the tank bottom. The agreement between experimental and simulation data in this region is satisfactory except when BC #3 was used. The results for $Z/H = 0.33$ show the effect of the presence of the impeller. Again, the agreement with the experimental data is better for the simulations based on BC #2 independently of the turbulence model used. In the portion of the vessel above the impeller

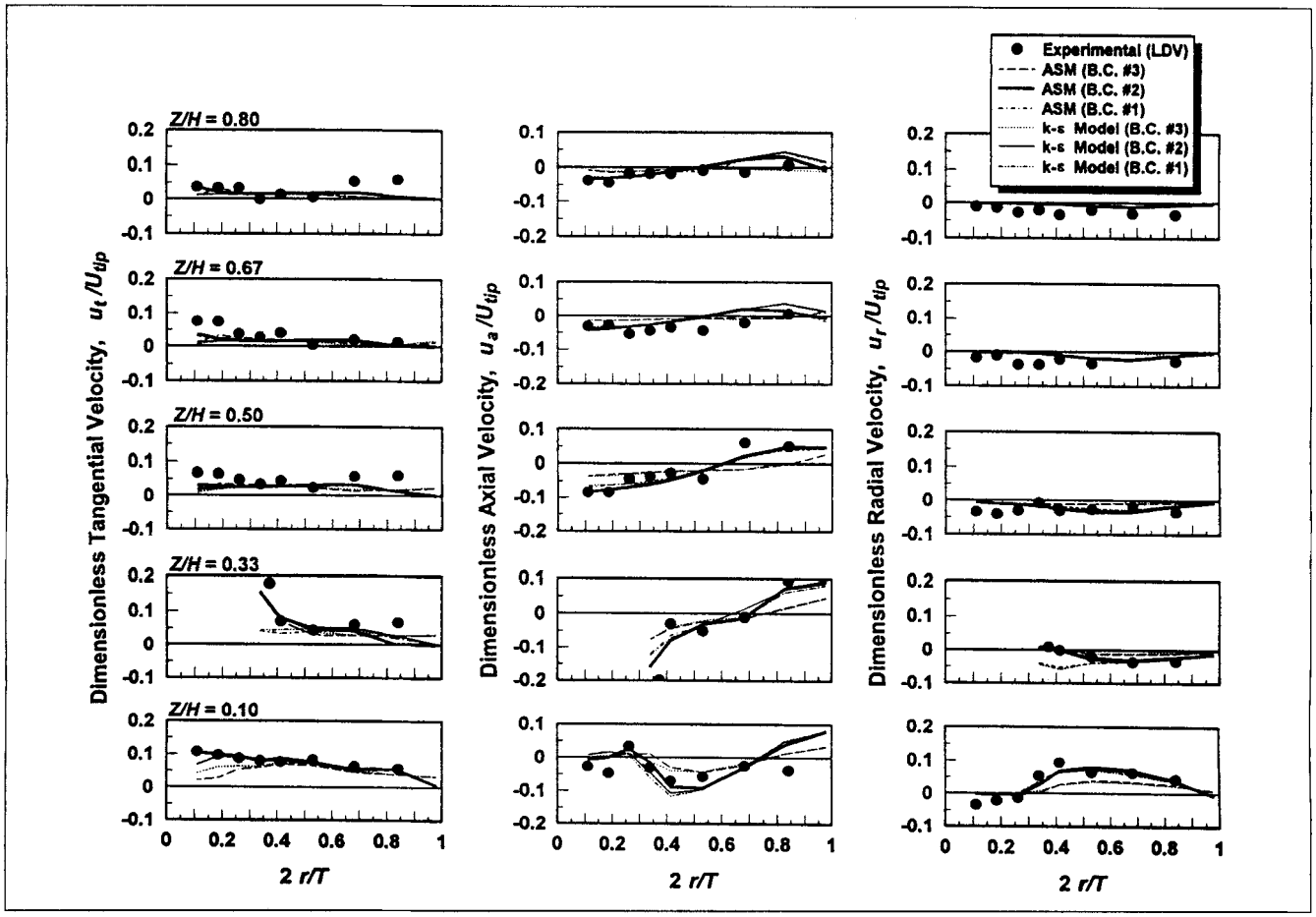

Figure 5. Experimental velocity measurements (via LDV) vs. numerical velocity predictions (via CFD) at five horizontal locations (Z/H) using different turbulence models (ASM and k-ϵ) and boundary conditions (BC #1, #2, and #3) for the single-PBT system.

Dimensionless tangential velocities (left figures). Dimensionless axial velocities (center figures). Dimensionless radial velocities (right figures).

the value of the tangential velocity is small and comparison between simulations and experimental data is more difficult.

Figure 5 shows that near the vessel bottom ($Z/H = 0.1$) the axial velocity is directed downwards for $2r/T > 0.3$, that is, in the region external to the impeller. Underneath the impeller the flow is close to zero, indicating the presence of a nearly stagnant zone. On the impeller plane the axial velocity is strongly oriented downwards near the impeller ($2r/T > 0.7$) and upwards otherwise. Above the impeller the flow is that typical of an axial impeller, that is, downwards in the center and upwards at the periphery of the tank. The simulation based on BC #2 and ASM is slightly superior to the others for any Z/H value.

A comparison between experimental and simulation results is also provided for the radial velocity component for the same Z/H values (Figure 5). Below the impeller a nearly stagnant zone can be again identified. Since the radial and the axial velocities in this zone are both close to zero, little exchange of fluid between this zone and the rest of the tank occurs. Only a swirling action is present in this zone because of the high values of the tangential component. On the impeller plane ($Z/H = 0.33$), the radial velocity is also quite modest since the flow is primarily directed downwards, at an angle. The simulations based on BC #2 are clearly superior to the others in this region. In the rest of the vessel the radial velocity is small and directed inwards to form a large recirculation loop above the impeller.

Figure 6 presents a comparison between the experimental dimensionless turbulent kinetic energies and the corresponding values produced using two simulations, both based on BC #2. It is difficult to determine which of the two turbulence models (ASM and k-ϵ) fits the results better. The values reported in this figure are smaller, in absolute terms, than the corresponding values produced by other investigators (Ranade et al., 1992; Kresta and Wood, 1993) for similar, but not identical systems, in which PBTs with larger blade width-to-impeller diameter ratios were used.

Figure 7 displays a contour plot of the power dissipated per unit volume. This plot shows that significant variations in the rate of power dissipations exist in the vessel. Near the impeller the power dissipation is predicted to be two or even three orders of magnitude larger than in the bulk of the vessels above the impeller. The contours in this figure appear rather similar, at least qualitatively, to those reported in the literature for a similar system (Ranade et al., 1989). The data from Figure 7 were used to calculate the total power dissipa-

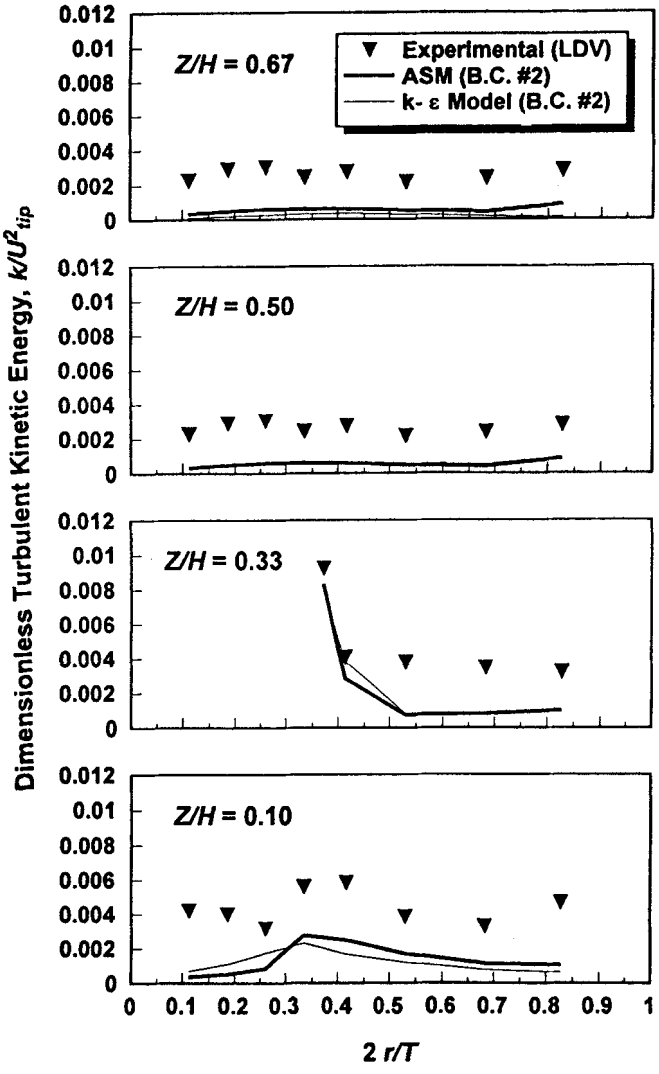

Figure 6. Experimental measurements (via LDV) vs. numerical predictions (via CFD) of the dimensionless turbulent kinetic energy at four horizontal locations (Z/H) using different turbulence models (ASM and k-ϵ) and BC #2.

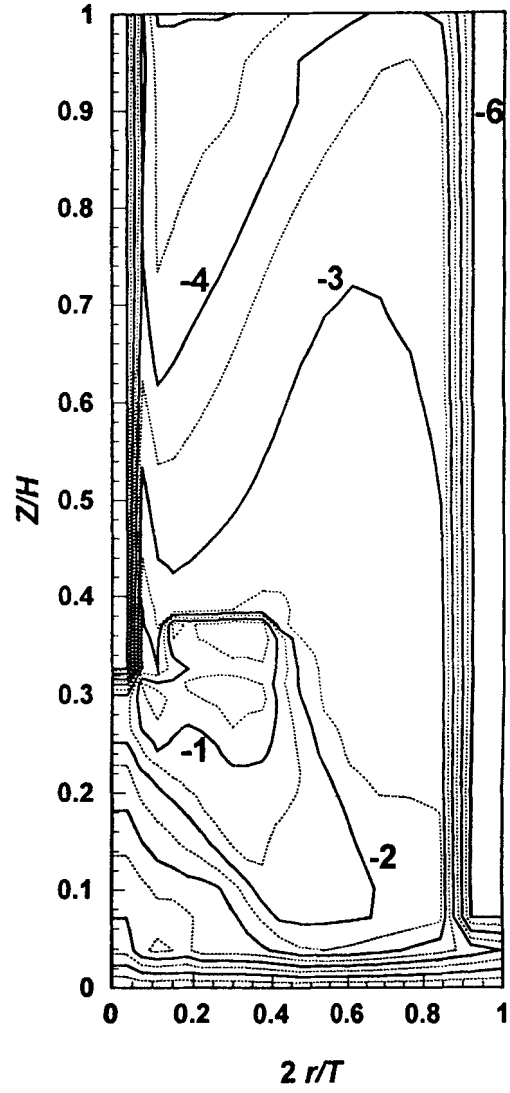

Figure 7. Numerical prediction of turbulence energy dissipation rates in the vertical plane between two baffles using ASM and BC #2 in the simulation.

Curve labels give the value of $\log_{10}(\epsilon)$, where ϵ is in m^2/s^3.

tion in the vessel by numerically integrating the expression:

$$P = \int_m \epsilon \, dm. \tag{11}$$

The value of P so calculated was found to be 0.206 W. This value was compared with the overall power consumption obtained from the direct measurement via strain gage, which was found to be equal to 1.826 W. Hence the ratio of computed power dissipation (from simulation) to experimental power dissipation (from direct torque measurement) was only 11.3%. The poor agreement between these two values cannot be attributed to the direct power dissipation measurement since the power number calculated this way was found to be 1.28, which is in close agreement with the value of 1.3 previously reported in the literature for a PBT having the same geometry (Bates et al., 1963, 1966). These results and the results for the turbulent kinetic energy indicate that the numerical simulation does not fully capture, quantitatively, some of the important features of the complex tridimensional flow in the vessel.

Finally, Figure 8 shows a tridimensional view of the velocity profiles obtained via simulation (Figure 8a), as well as a bidimensional cross-sectional view of the same velocities on a plane passing through the impeller shaft (Figure 8b). From these figures one can clearly see the typical top-to-bottom main circulation pattern associated with PBT-generated flows and the presence of a nearly stagnant zone under the impeller (as far as the velocities in the cross-sectional plane are concerned).

The results obtained here for a single PBT can be partially compared with the results obtained in the literature for other PBT systems (Ranade and Joshi, 1989; Jaworski et al., 1991; Ranade et al., 1992; Kresta and Wood, 1993b; Armenante et

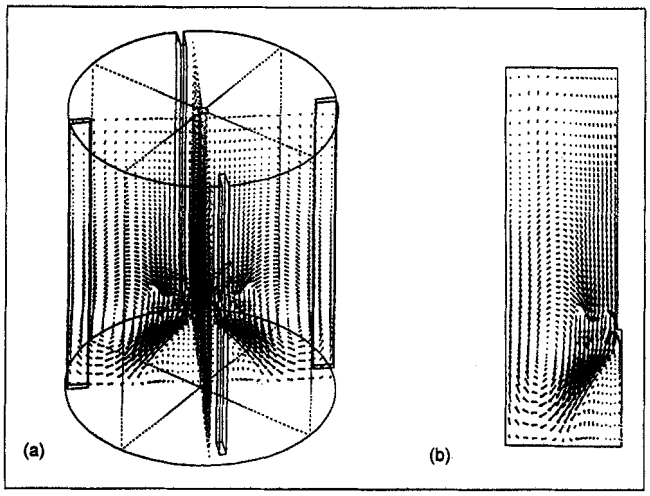

Figure 8. CFD prediction of velocity distribution in the single-PBT agitation system using BC #2 and ASM.

(a) Tridimensional view. (b) Bidimensional cross section across the impeller shaft (only one half section shown).

al., 1994). The tangential velocities obtained here for $Z/H = 0.1$ can be approximately compared with those of Ranade et al. (1989), who examined the case for which Z/H is equal to 0.668, 0.015, and 0.233, respectively. Their nondimensional tangential velocity for the lowest of these Z/H values is of the order of 0.1, which is quite similar to the value found here. However, their curve shows a moderate peak for $2r/T = 0.38$ that is absent in the present study. More pronounced peaks appear in their other curves for higher Z/H values. Kresta and Wood (1993b) also produced several curves for the tangential velocities below the impeller. The curve that is closest to the Z/H value used here (0.1) is that for which $Z/H = 0.192$. This curve also shows a peak ($u_t/U_{tip} = 0.2$) for $2r/T \approx 0.27$. A possible explanation for the discrepancies between tangential velocities near the vessel bottom is in the difference in baffling system, which extends all the way to the bottom of the vessel in the case of these two studies in the literature, but not in this study. In fact, the profile found in the present study is rather similar to that observed in a similar but closed, unbaffled vessel agitated by a PBT (Armenante et al., 1994). However, the tangential velocity on the same plane of the impeller was found here to have a marked upward trend near the impeller tip, similar to the velocity profiles found by other investigators on planes under the impeller (Ranade and Joshi, 1989; Kresta and Wood, 1993b). In particular, the values of u_t/U_{tip} for $2r/T > 0.33$ just below the impeller were found to be very close to those of Kresta and Wood (1993b). Comparisons of the tangential velocities above the impeller with other results in the literature are difficult to make because of lack of data.

The results obtained here for the axial velocities can only be qualitatively compared with the results of previous literature studies because of the differences in the geometries of the impeller and the baffles. Ranade and Joshi (1989) produced axial velocity profiles for the region below the impeller that are similar to that shown in Figure 5 for $Z/H = 0.1$. As observed previously, the numerical values of the peaks in their u_a/U_{tip} curves are greater than that found here (0.25 vs. 0.12). However, the impeller they used had a much larger w/D ratio than that used here (1/5 vs. 1/8). A similar argument can be used to interpret the data of Jaworski et al. (1991), and Kresta and Wood (1993b), which also show numerical results similar to those of Ranade and Joshi (1989). The curves that the latter authors obtained for the region above the impeller also agree qualitatively with the curves produced here for Z/H equal to 0.5, 0.67, and 0.8.

Previous investigations have shown that the radial component is typically quite small anywhere in the vessel except for the region below the impeller. This is what was found here as well (Figure 5). Significant agreement between the result of this work and the data of Jaworski et al. (1991) and Kresta and Wood (1993b) was found. The data of the former workers indicate that the radial velocity is small and directed inwards above the impeller and outwards below the impeller, except for the region just under it. This is precisely what was observed here (Figure 5). As before, the major difference between data in the literature and the data of the present work is in the magnitude of the velocities, which is lower here, possibly because of the smaller impeller blade width. The data of Ranade and Joshi (1989) for u_r are also in overall qualitative agreement with the data of this study.

Double-impeller configuration

Velocities in the Impeller Regions. The experimentally determined velocities in the upper impeller and lower impeller regions are given in Figures 9 and 10, respectively. As for the single-PBT system the axial velocities were all directed downwards. A comparison between these two figures reveals that the axial velocities on the top surfaces of both impellers are identical for $r/R > 0.7$. For $r/R < 0.7$ the top-layer velocity of the lower impeller is nearly flat, while that of the upper impeller decreases, in absolute value, toward zero as the ratio r/R becomes smaller. The velocity on the bottom surface of the lower impeller was found to be slightly but consistently higher than the corresponding velocity for the upper impeller. These results indicate that the pumping action of the upper impeller produces a stronger and more homogeneous downward flow across the lower impeller. An examination of Figure 10 and Figure 3 provides a comparison between the velocities in the same (lower) impeller region in the presence or absence of the upper impeller. The axial velocity profiles for both the top and bottom surfaces appear nearly the same with or without the upper impeller. However, the presence of the upper impeller produces a more constant and smooth axial velocity profile. This is probably the result of a more directionally homogeneous inflow to the lower impeller resulting from the presence of the upper impeller. By comparing Figure 9 (for the upper impeller) with Figure 3 (for the single impeller) one can see that the axial velocity profiles on the top surfaces have nearly identical shapes, but that the curve for the upper impeller appears translated toward the right. This is probably the result of the shorter distance between the upper impeller and the free liquid surface (compared to the single-impeller case), which forces the upward flow near the vessel wall to turn inward (i.e., toward the center of the vessel) as it approaches the free surface, and then downward near the center of the vessel (to feed the suction side of the

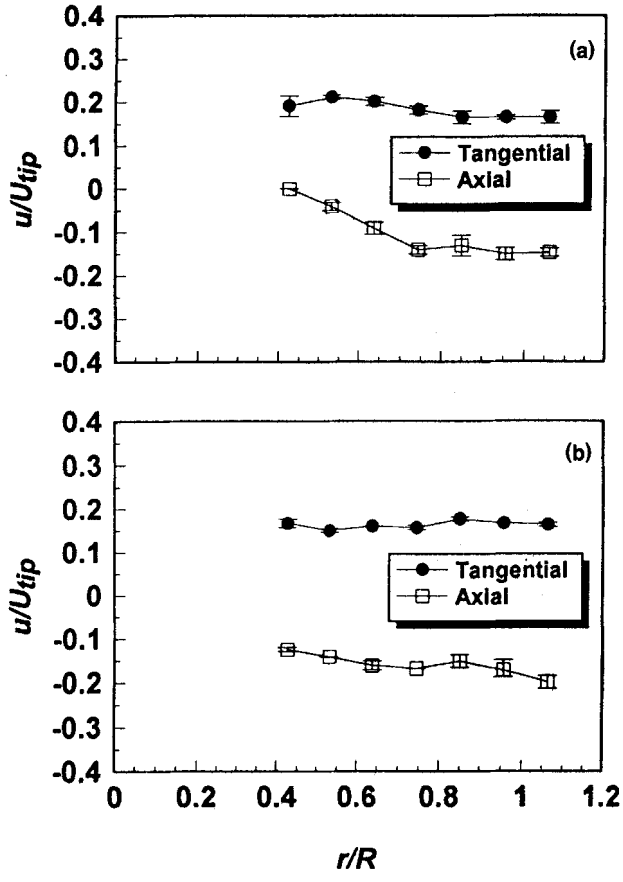

Figure 9. Experimentally determined (via LDV) dimensionless velocities in the upper impeller region for the double PBT system.

(a) Velocities at the top plane of the volume swept by the upper impeller. (b) Velocities at the bottom plane of the volume swept by the upper impeller. Positive values indicate upward velocities (for the axial direction). Error bars indicate standard deviation of duplicate experiments. These velocity values were used as boundary conditions in the CFD simulations (see text).

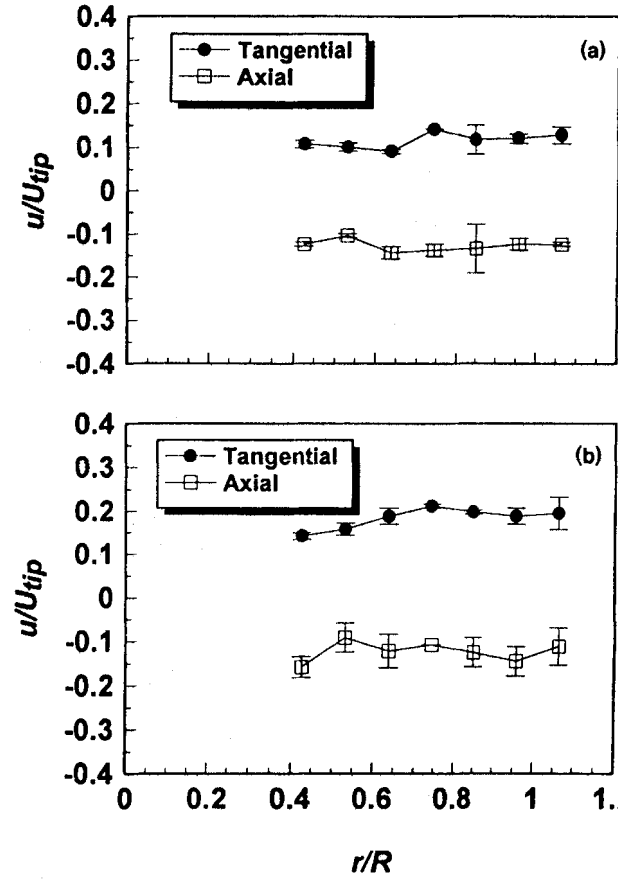

Figure 10. Experimentally determined (via LDV) dimensionless velocities in the lower impeller region for the double PBT system.

(a) Velocities at the top plane of the volume swept by the lower impeller. (b) Velocities at the bottom plane of the volume swept by the lower impeller. Positive values indicate upward velocities (for the axial direction). Error bars indicate standard deviation of duplicate experiments. These velocity values were used as boundary conditions in the CFD simulations (see text).

impeller) in a much shorter vertical distance in the upper-impeller case than in the single-impeller case. This more rapid change in flow direction produces a small but detectable short-circuiting effect in the region above the upper impeller, resulting in a decrease in axial downward flow near the center of the vessel. This, in turn, produces a "shift to the right" in the axial velocity profile above the upper impeller, compared to the single-impeller case. A similar comparison for the bottom surfaces shows that the axial velocities are very similar but that the profile for the upper impeller is smoother than that of the single impeller, probably because of the presence of the lower impeller, which makes the flow between the upper and lower impeller more axially oriented.

Figures 9 and 10 also reveal that the tangential velocity profiles on the bottom faces of the upper and lower impellers are practically identical. However, a similar comparison for the top surfaces indicates that the tangential velocities for the upper impeller are noticeably higher than the corresponding velocities for the lower impeller. This is somewhat counterintuitive since one would expect that a stronger tangential flow in the neighborhood of the lower impeller would be generated in the presence of the upper impeller rather than in its absence. On the other hand, a comparison of Figure 9 (for the upper impeller) with Figure 3 (for the single impeller) shows that the tangential velocities on both the top and bottom surfaces are virtually superimposable. This confirms that the flow in the upper impeller region is similar to that observed in a single-impeller region. A likely explanation for this is in the weak flow (especially tangential flow) generated by a PBT in the vessel region above the impeller (as shown in Figure 8) that makes the flow near the upper impeller largely (although not completely) independent of the flow field generated by the lower impeller.

The values of the turbulent kinetic energy at the top and bottom surfaces of the upper-impeller and lower-impeller regions were calculated from the three components of the fluctuating velocities and are shown in Figures 11 and 12, respectively. A significant difference exists between the k/U_{tip}^2 profiles for the two regions. In particular, the k/U_{tip}^2 profile for the top surface of the upper impeller was found to be significantly lower than that for the top surface of the lower impeller. On the other hand, a comparison between Figure 4a

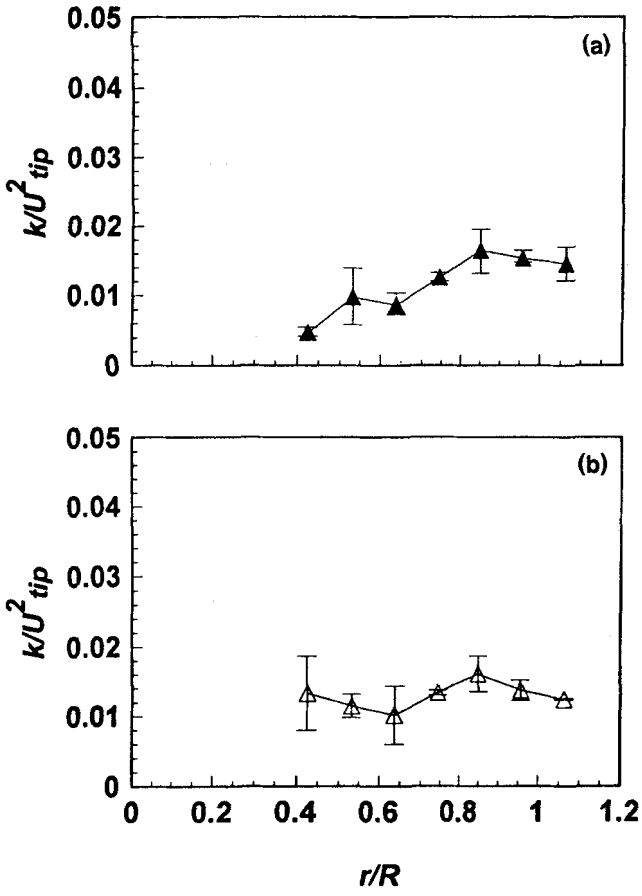

Figure 11. Experimentally determined (via LDV) dimensionless turbulent kinetic energies in the upper impeller region for the double PBT system.

(a) Kinetic energies at the top plane of the volume swept by the upper impeller. (b) Kinetic energies at the bottom plane of the volume swept by the upper impeller. Error bars indicate standard deviation of duplicate experiments. These kinetic-energy values were used as boundary conditions in the CFD simulations (see text).

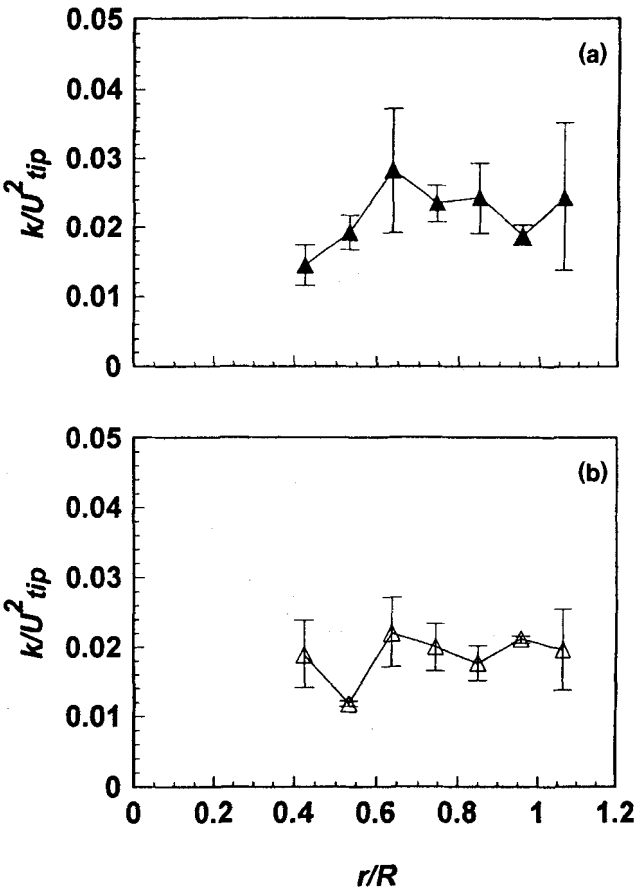

Figure 12. Experimentally determined (via LDV) dimensionless turbulent kinetic energies in the lower impeller region for the double PBT system.

(a) Kinetic energies at the top plane of the volume swept by the lower impeller. (b) Kinetic energies at the bottom plane of the volume swept by the lower impeller. Error bars indicate standard deviation of duplicate experiments. These kinetic-energy values were used as boundary conditions in the CFD simulations (see text).

and Figure 11a shows no appreciable differences between the top surface k/U^2_{tip} values for the single impeller case and those for the upper impeller case. This indicates that the turbulent flow generated by the upper impeller travels downwards, resulting in a higher level of turbulence on the top face of the lower impeller. An appreciable difference also exists between the k/U^2_{tip} values on the bottom surfaces of the upper and lower impellers (Figures 11b and 12b), although not as pronounced as in the top surface case. By comparing Figures 4b, 11b and 12b, one can see that the bottom surface k/U^2_{tip} values are rather similar for the single-impeller and upper-impeller case, but not for the lower-impeller case. This again confirms that whereas the upper impeller has a significant impact on the flow and turbulence level in the lower-impeller region, the reverse is not true, and that the upper impeller is quite similar to a single impeller as far as flow and turbulence in the impeller region are concerned.

Velocities Outside the Impeller Regions. Figure 13 shows the velocity profiles in the bulk of the liquid for the double PBT agitation system at five different horizontal planes. Examination of this figure reveals that, in general, the experimental LDV data and the results of the CFD simulations in which the velocity and turbulent kinetic energy profiles in the impeller regions (Figures 9, 10, 11, and 12) were used as boundary conditions follow the same trends. Only BC #2 was used in the simulations for the double PBT system, since the simulations based on this boundary condition proved to be superior to the others for the single-impeller case. However, both turbulence models (k-ϵ and ASM) were used.

As in the single-PBT case, the tangential velocity near the vessel bottom ($Z/H = 0.1$) was found to be relatively constant, although significantly smaller in value (about 50%) than in the former case. This is somewhat counterintuitive since one would expect that the presence of a second impeller would reinforce the flow near the vessel bottom, including the tangential component. The tangential velocity profile for $Z/H = 0.33$ is clearly affected by the presence of the impeller on the same plane, and is very similar to the corresponding single-PBT case. However, the velocity profile in the middle

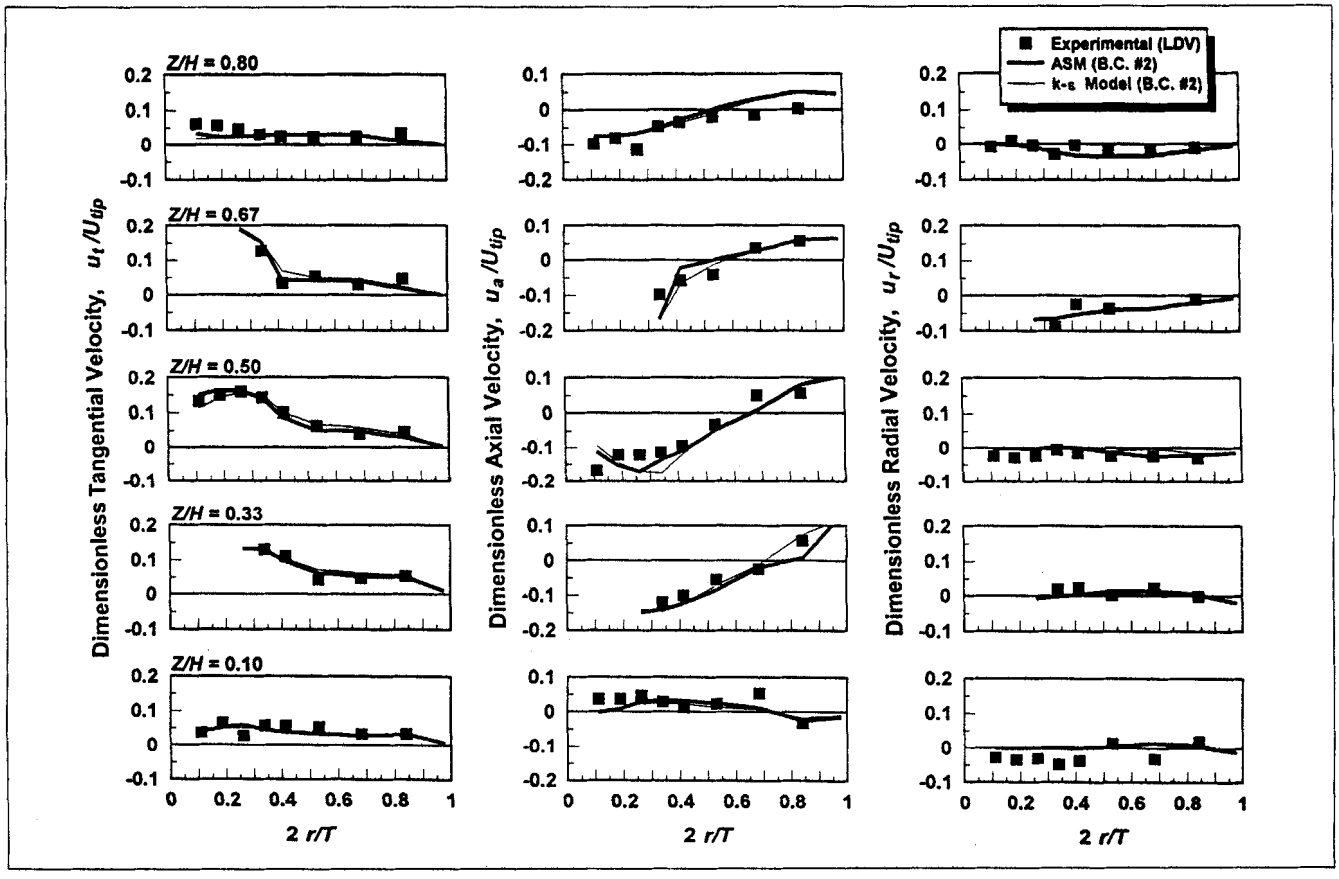

Figure 13. Experimental velocity measurements (via LDV) vs. numerical velocity predictions (via CFD) at five horizontal locations (Z/H) using different turbulence models (ASM and k-ϵ) and boundary condition BC #2 for the double PBT system.

Dimensionless tangential velocities (left figures). Dimensionless axial velocities (center figures). Dimensionless radial velocities (right figures).

of the vessel ($Z/H = 0.5$) is substantially higher in this case, probably because of the upper impeller. The tangential velocity profile at $Z/H = 0.67$ is similar to that at $Z/H = 0.33$, and even more similar to that of a single PBT also at $Z/H = 0.33$. Finally, the profile in the upper region ($Z/H = 0.8$) shows that the tangential velocities above the impeller are only moderately affected by the proximity of the upper impeller and are only slightly higher than the corresponding values for the single-PBT case. In any case, the curves in these figures indicate that no significant difference exists between the predictions based on the two turbulence models.

The results reported in Figure 13 show that the presence of the upper impeller has a significant impact on the axial flow throughout the vessel. The most dramatic evidence of this can be seen near the bottom of the vessel. A comparison between Figures 13 and 5 for $Z/H = 0.10$ shows that the axial flow is now directed upwards in the central bottom part of the vessel ($2r/T < 0.7$), and downwards near the vessel wall. This is almost exactly the reverse of the flow produced by a single PBT. While the axial flow in the lower impeller region ($Z/H = 0.33$) is similar to that for a single impeller (Figure 5), the axial velocities between the impellers ($Z/H = 0.50$) are significantly larger in the central vessel region for the case of a double PBT system, which is what one could intuitively anticipate. The axial flow in the upper impeller region ($Z/H = 0.67$) and in the region above that ($Z/H = 0.80$) are clearly affected by the presence of the upper impeller.

As for the radial velocities, significant differences exist between the double PBT and single-PBT cases in the region near the vessel bottom ($Z/H = 0.10$) where the flow intensity is much lower in the former case. Also, in the region of the lower impeller ($Z/H = 0.33$) the radial flow is directed outwards in the double PBT case and inward in the single-PBT case. In the rest of the vessel no appreciable differences between the two configurations can be seen, except for the region where the upper impeller is ($Z/H = 0.67$).

Finally, the simulated flow pattern generated by two PBTs is given in Figure 14. A comparison of this figure with the corresponding figure for the single impeller configuration (Figure 8) shows the striking differences in flow pattern resulting from the presence of the second impeller. The main top-to-bottom axial flow is clearly stronger, especially between the two impellers. More significantly, the angled discharge from the bottom impeller is now deflected horizontally before reaching the bottom of the vessel. This produces an expansion of the low circulation region previously observed just under the impeller in the single-PBT case, and results in the entire bottom region in the vessel being almost

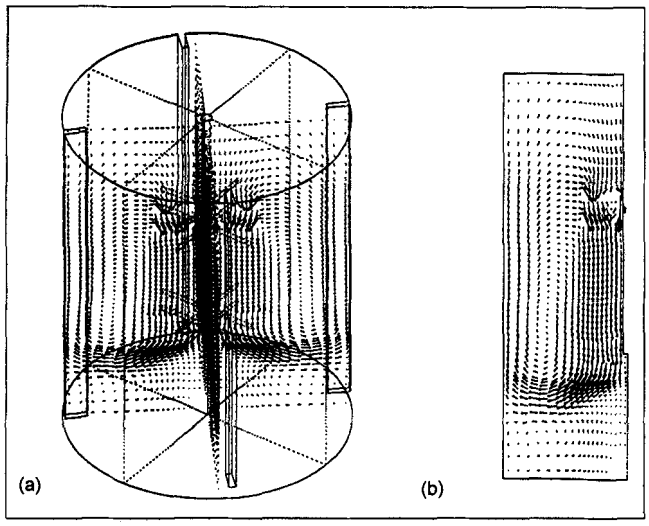

Figure 14. CFD prediction of velocity distribution in the double PBT agitation system using BC #2 and ASM.

(a) Tridimensional view. (b) Bidimensional cross section across the impeller shaft (only one half section shown).

completely cut off from the main circulation loop. In fact, a secondary recirculation loop can be observed in the region located between the vessel bottom and the wall.

This change in flow pattern is not only counterintuitive but can also have dramatic consequences on some of the typical industrial applications of PBTs, such as the off-bottom suspension of solid particles. Contrary to what one may expect, the addition of a second impeller is likely to have (at least in this case) a negative impact on the suspension ability of the agitation system. This would not only result in a higher agitation speed to achieve the same degree of solid suspension, but also in a much higher power consumption caused by the presence of the second impeller. A situation of this kind has been already described in the literature. For example, Armenante et al. (1992) have already observed that the presence of two or three impellers instead of one may sometimes result in higher agitation speeds and higher power consumptions to achieve the same complete particle suspension state in solid–liquid systems (N_{js}), or the complete dispersion state in liquid–liquid systems (N_{cd}). This phenomenon was observed only for certain values of the impeller spacing. However it was not limited to mixed-flow impellers only, such as PBTs, but was also observed with radial flow impellers, such as disk turbines and flat-blade turbines (Armenante et al., 1992; Armenante and Li, 1993).

The results of the current work were obtained for only one value of the spacing between impellers. Therefore it is difficult to speculate on whether the presence of a second impeller would consistently and significantly alter the flow produced by the first impeller. However, indirect evidence from the work on solid suspension and liquid dispersion cited earlier, as well as data from power measurements (Bates et al., 1963, 1966; Hudcova et al., 1989) and mixing time (Mahmoudi and Yianneskis, 1991) indicate that this is not the case, and that significant interference between the two primary flows generated by the impellers occurs only for specific values of the impeller spacing (typically for $S/D \approx 1$–1.5) When the impellers are quite far apart, it is likely the flow pattern of dual-impeller systems becomes similar to that generated by two individual single impellers, while when the impellers are very close to each other, the flow is similar to that of a single impeller.

Conclusions

In this article numerical predictions based on CFD simulations and LDV experimental values of the tridimensional velocity profiles in baffled vessels agitated with one or two PBTs were presented. Better predictions were obtained if the boundary conditions used in the simulation were specified at two rather than one of the surfaces of the region swept by the impeller(s). However, specifying the boundary conditions around all the impeller surfaces did not produce any improvement. Instead poorer agreement was found. The reason for this is likely to be the sensitivity of the simulation program to small errors in the mass balance around the impeller (completely defined when this set of boundary conditions is used), and hence the difficulty of the program to converge to a stable solution during successive iterations. Of the two turbulence models used in this work—ASM and k-ϵ—the former produced results in marginally but consistently better agreement with the experimental data than the latter.

The results for the single impeller configuration indicate that the flow is dominated by the axial component of the velocity, resulting in a major top-to-bottom recirculation loop characteristic of single-PBT flow in mixing vessel. The introduction of a second impeller produced a significant shift in the flow pattern, generating an even stronger axial recirculation loop in the central and upper part of the vessel, but also creating a secondary recirculation loop in the lower part of the vessel completely extending over the entire bottom of the vessel. Because of the low velocities observed in this secondary loop, mixing in this region is likely to be poor. This could result in a significant and negative impact of the presence of the second impeller on phenomena such as off-bottom solid suspension, which strongly depends on the velocity profiles and turbulence intensity in the region near the vessel bottom. Hence, caution should be observed when an additional PBT is added to a single PBT in order to improve the mixing performance of the system.

Acknowledgment

This work was partially supported by the National Science Foundation (grant No. EEC-9520573) and the Exxon Education Foundation (thanks to the interest of Ramesh R. Hemrajani of Exxon Research and Engineering) whose contribution is gratefully acknowledged.

Notation

C = impeller clearance off the vessel bottom, m
D = impeller diameter, m
G_k = generation of turbulence kinetic energy, k; kg/m·s^3
H = height of liquid in mixing vessel, m
k = specific turbulence kinetic energy, m^2/s^2
m = mass of liquid in vessel, kg
N = agitation speed, rotation/s
p = variable defined by Eq. 2
p_{ij} = variable defined by Eq. 2
Q = impeller discharge flow rate, m^3/s

r = radial distance from vessel centerline, m
R = radius of impeller, m
S = spacing between impellers, m
T = vessel diameter, m
u = velocity, m/s
$\boldsymbol{u}$ = velocity vector, m/s
u_r = radial velocity, m/s
u_t = tangential velocity, m/s
u_z = axial (vertical) velocity, m/s
$\bar{\boldsymbol{u}}$ = time-averaged velocity vector, m/s
$\boldsymbol{u}'$ = fluctuating velocity vector, m/s
u_i' = fluctating velocity in the ith direction; m/s
U_{tip} = impeller tip velocity; m/s
w = vertically projected width of impeller blade, m
x_i, x_j, x_l = coordinate variables, m
Z = axial (vertical) distance from vessel bottom, m

Greek letters

α = constant used during the numerical simulation of turbulence (Eq. 8), nondimensional
δ_{ij} = Kronecker delta
μ_t = turbulent viscosity, kg/(m·s)
ρ = liquid density, kg/m^3
σ_k = constant used during the numerical simulation of turbulence, nondimensional
σ_ϵ = constant used during the numerical simulation of turbulence, nondimensional

Literature Cited

Armenante, P. M., and C. C. Chou, "Experimental LDV Measurement and Numerical CFD Determination of the Fluid Velocity Distribution in an Unbaffled Mixing Vessel," *AIChE Symp. Ser.*, **90**(299), 33 (1994).

Armenante, P. M., C. C. Chou, and R. R. Hemrajani, "Comparison of Experimental and Numerical Fluid Velocity Distribution Profiles in an Unbaffled Mixing Vessel Provided with a Pitched-Blade Turbine," *I. Chem. Eng. Symp. Ser.*, No. 136, Cambridge, U.K., 21 (1994).

Armenante, P. M., Y.-T. Huang, and T. Li, "Determination of the Minimum Agitation Speed to Attain the Just Dispersed State in Solid-Liquid and Liquid-Liquid Reactors Provided with Multiple Impellers," *Chem. Eng. Sci.*, **47**, 2865 (1992).

Armenante, P. M., and T. Li, "Minimum Agitation Speed for Off-Bottom Suspension of Solids in Agitated Vessels Provided with Multiple Flat-Blade Impellers," *AIChE Symp. Ser.*, **89** (293), 105 (1993).

Bakker, A., "Hydrodynamics of Stirred Gas-Liquid Dispersions," PhD Diss., Delft Univ. of Technology, Delft, The Netherlands (1992).

Bates, R. L., P. L. Fondy, and R. R. Corpstein, "An Examination of Some Geometric Parameters of Impeller Power," *Ind. Eng. Chem. Proc. Des. Dev.*, **2**, 310 (1963).

Bates, R. L., P. L. Fondy, and J. C. Fenic, "Impeller Characteristics and Power," *Mixing: Theory and Practice*, Vol. I, V. W. Uhl and J. B. Gray, eds., Academic Press, New York (1966).

Costes, J., C. Alran, and J. P. Couderc, "Characteristics of the Discharge Flow from a Rushton Turbine. Measurements by Thermal and Laser-Doppler Anemometry," *Int. Chem. Eng.*, **31**, 55 (1991).

Creare.x, Inc., *FLUENT—Computational Fluid Dynamics Software User's Manual*, Hanover, NH (1990).

de Groot, P. J., "LDA Used to Check Nagata's Model for Vortex Geometry in Stirred Vessels," *Laser Anemom. Int. Conf. (ASME)*, Vol. 1, p. 247 (1991).

Dyster, K., Z. Jaworski, E., Koutsakos, and A. W. Nienow, "An LDA Study of the Radial Discharge Velocities Generated by a Rushton Turbine: Newtonian Fluids, $Re \geq 5$," *Trans Inst. Chem. Eng., Part A, Chem. Eng. Res. Des.*, **71**, 11 (1993).

Fort, I., "Flow and Turbulence in Vessels with Axial Impellers," in *Mixing: Theory and Practice*, Vol. III, V. W. Uhl and J. B Gray, eds., Academic Press, New York, (1986).

Gray, J. B., "Flow Patterns, Fluid Velocities, and Mixing in Agitated Vessels," *Mixing: Theory and Practice*, Vol. I, Uhl, V. W. and J. B. Gray, eds., Academic Press, New York (1966).

Hirata, Y., A. W. Nienow, and I. P. Moore, "LDA Studies of Velocity Distributions and Cavern Sizes in a Yield Stress Fluid Agitated by a Rushton Turbine," *Proc. Eur. Conf. on Mixing, Brugge (Belgium)*, Vol. 1, p. 167 (1991).

Hudcova, V., V. Machon, and A. W. Nienow, "Gas-Liquid Dispersion with Dual Rushton Turbine Impellers," *Biotechnol. Bioeng.*, **34**, 617 (1989).

Jaworski, Z., A. W. Nienow, E. Koutsakos, K. Dyster, and W. Bujalski, "An LDA Study of Turbulent Flow in a Baffled Vessel Agitated by a Pitched Blade Turbine," *Trans. Inst. Chem. Eng., Part A, Chem. Eng. Res. Des.*, **69**, 313 (1991).

Kresta, S. M., and P. E. Wood, "Prediction of the Three-Dimensional Turbulent Flow in Stirred Tanks," *AIChE J.*, **37**(3), 448 (1991).

Kresta, S. M., and P. E. Wood, "The Flow Field Produced by a Pitched Blade Turbine: Characterization of the Turbulence and Estimation of the Dissipation Rate," *Chem. Eng. Sci.*, **48**, 1761 (1993a).

Kresta, S. M., and P. E. Wood, "The Mean Flow Field Produced by a 45° Pitched Blade Turbine: Changes in the Circulation Pattern Due to Off Bottom Clearance," *Can. J. Chem. Eng.*, **71**, 42 (1993b).

Launder, B. E., and D. B. Spalding, *Mathematical Models of Turbulence*, Academic Press, London (1972).

Luo, J. Y., A. D. Gosman, R. I. Issa, J. C. Middleton, and M. K. Fitzgerald, "Full Flow Field Computation of Mixing in Baffled Stirred Vessels," *Chem. Eng. Res. Des.*, **71**, 342 (1993).

Mahmoudi, S. M., and M. Yianneskis, "The Variation of Flow Pattern and Mixing Time with Impeller Spacing in Stirred Vessels with Two Rushton Impellers," *Proc. Eur. Conf. on Mixing*, Vol. 1, Brugge, Belgium, p. 17 (1991).

Mahouast, M., G. Cognet, and R. David, "Two-Component LDV Measurement in a Stirred Tank,," *AIChE J.*, **35**, 1770 (1989).

Oldshue, J. Y., *Fluid Mixing Technology*, McGraw-Hill, New York (1984).

Ranade, V. V., and J. B. Joshi, "Flow Generated by Pitched Blade Turbines: I. Measurements Using Laser Doppler Anemometer," *Chem. Eng. Comm.*, **81**, 197 (1989).

Ranade, V. V., and J. B. Joshi, "Flow Generated by a Disc Turbine: I. Experimental," *Chem. Eng. Res. Des.*, **68**, 19 (1990a).

Ranade, V. V., and J. B. Joshi, "Flow Generated by a Disc Turbine: II. Mathematical Modelling and Comparison with Experimental Data," *Chem. Eng. Res. Des.*, **68**, 34 (1990b).

Ranade, V. V., J. B. Joshi, and A. G. Marathe, "Flow Generated by Pitched Blade Turbines: II. Simulation Using k-ϵ Model," *Chem. Eng. Commun.*, **81**, 225 (1989).

Ranade, V. V., V. P. Mishra, V. S. Saraph, G. B. Deshpande, and J. B. Joshi, "Comparison of Axial Flow Impellers Using a Laser Doppler Anemometer," *Ind. Eng. Chem. Res.*, **31**, 2370 (1992).

Rewatkar, V. B., K. S. M. S. Raghava Rao, and J. B. Joshi, "Power Consumption in Mechanically Agitated Contractors Using Pitched Bladed Turbine Impellers," *Chem. Eng. Commun.*, **88**, 69 (1990).

Rodi, W., *Turbulent Models and Their Application in Hydraulics—A State of Art Review*, 2nd ed. International Association for Hydraulic Research, Delft, The Netherlands (1984).

Weetman, R. J., "Development of Transitional Flow Mixing Impeller," *Proc. Eur. Conf. on Mixing*, Brugge, Belgium, Vol. 1, p. 25 (1991).

Wu, H., and G. K. Patterson, "Laser-Doppler Measurements of Turbulent-Flow Parameters in a Stirred Mixer," *Chem. Eng. Sci.*, **44**, 2207 (1989).

Manuscript received June 30, 1994, and revision received Feb. 22, 1995.